Computational Study of Room Temperature Molten Salts Composed by 1-Alkyl-3-methylimidazolium CationsForce-Field Proposal and Validation

ARTICLE *in* THE JOURNAL OF PHYSICAL CHEMISTRY B · NOVEMBER 2002

Impact Factor: 3.3 · DOI: 10.1021/jp0216629

3 AUTHORS, INCLUDING:

Elvis Boes
Federal Institute of Education, Science and T…
10 PUBLICATIONS **443** CITATIONS
SEE PROFILE

Hubert Stassen
Universidade Federal do Rio Grande do Sul
55 PUBLICATIONS **836** CITATIONS
SEE PROFILE

Computational Study of Room Temperature Molten Salts Composed by 1-Alkyl-3-methylimidazolium Cations—Force-Field Proposal and Validation

Jones de Andrade, Elvis S. Böes, and Hubert Stassen*

Grupo de Química Teórica, Instituto de Química, Universidade Federal do Rio Grande do Sul, 91540-000 Porto Alegre - RS, Brazil

Received: July 18, 2002; In Final Form: October 21, 2002

We present a complete force field for liquid-state simulations on ionic liquids containing 1-ethyl-3-methylimidazolium and 1-*n*-butyl-3-methylimidazolium cations and the tetrachloroaluminate and tetrafluoroborate anions. The force field is compatible with the AMBER methodology and is easily extendable to other dialkylimidazolium salts. On the basis of the general AMBER procedures to develop lacking intramolecular parameters and the RESP approach to calculate the atomic point charges, we obtained an all-atom force field which was validated against the experimental density, diffusion coefficient, vibrational frequencies, as well as X-ray (crystal state) and neutron (liquid state) diffraction structural data. Moreover, molecular mechanics calculations for the developed force field produce the cation's structures and dipole moments in very good agreement with quantum mechanical ab initio calculations. In addition, a basic study concerning the simulated liquid structure in terms of the radial distribution functions has been undertaken using molecular dynamics simulation. In summary, we achieved a very consistent picture in the computed data for the four room-temperature molten salts.

1. Introduction

In the past decades, both the public concern and the rigorous legislations on the environmental awareness and the protection of natural resources lead the chemistry to invest in the so-called green technologies.[1] As an example, one might cite the search for alternatives to the common organic solvents being substituted by supercritical fluids,[2] perfluorinated solvents,[3] or room-temperature molten salts (RTMS).[4]

The RTMS represent an interesting solvent class for the following reasons:[5] (i) They are almost nonvolatile avoiding the first and basic contamination problems. (ii) They represent very good solvents for a broad class of organic and inorganic materials and are very stable against strong reaction medias. (iii) Their bicomponent phase diagrams together with supercritical carbon dioxide (another green solvent) are published enabling biphasic catalysis with these two solvents. (iv) Although the RTMS are polar solvents, most of them are immiscible with water or present a very low hygroscopicity. (v) Despite their polarity, RTMS are composed of poor coordinating ions, which can be used to enhance chemical reactions carried out in them. Because of all these interesting and unique properties, the number of experimental studies on RTMS has grown enormously in recent years.

On the other hand, only few computational or theoretical studies on such systems are described in the literature. One might mention four quantum mechanical (QM) studies on isolated ions or molecules,[6−8] and very recently, studies focusing on liquid-state characteristics by molecular dynamics (MD)[9−11] and Monte Carlo[12] computer simulations appeared in the literature. These theoretical studies have been dedicated to the RTMS containing dialkylimidazolium type cations.

A huge problem faced in the study of RTMS systems by classical approaches is the lack of a complete force field which can well describe the liquid phase. In ref 9, a force field for non-RTMS based on dialkylimidazolium cations has been used to explore some structural aspects of these ionic liquids. Thermodynamic properties of dialkylimidazolium type RTMS have been calculated from a united atom force field.[12] However, X-ray crystal data on various dialkylimidazolium salts[13,14] reveal the existence of hydrogen bonds between the anions and hydrogens of the imidazolium ring. The united atom approach might be less accurate than an all-atom approach, especially in predicting hydrogen bonds that might be very important for the associative character between the ions in RTMS. For this reason, in a preliminary communication,[10] we have established an all-atom force field for the RTMS 1-ethyl-3-methylimidazolium tetrachloroaluminate reproducing several experimental properties for this particular ionic liquid.

In this paper, we report more details of the force field introduced in ref 10 as an extension to the AMBER force field[15] and present additional results for the RTMS based on dialkylimidazolium cations. Therefore, we treat an important class of RTMS: 1-ethyl-3-methylimidazolium (EMI) and 1-*n*-butyl-3-methylimidazolium (BMI) cations with tetrachloroaluminate and tetrafluoroborate anions. The force field development followed most of AMBER's algorithmic protocol.[16] All of the potential parameters have been established in such a way that they can easily be adapted to other RTMS containing dialkylimidazolium cations.

The methodological self-consistency has motivated us to choose the AMBER force field that is rather independent of experimental input. Because of their extremely low volatile character, experimental values for the heat of vaporization are not accessible for the RTMS. Thus, adjusting potential parameters with respect to simple thermodynamic properties (internal energy, heat of vaporization) is an impossible task for the ionic liquids. We have performed QM studies on the isolated ions in order to obtain optimized geometries and charge distributions that were used to establish both, intramolecular potential

* To whom correspondence should be addressed. E-mail: gullit@iq.ufrgs.br.

10.1021/jp0216629 CCC: $22.00
Published on Web 11/23/2002

parameters and atomic point charges. In a second step, these parameters were used to explore the molecular configuration space of the isolated ions by molecular mechanics (MM) calculations, before applying the complete force field with additional intermolecular parameters for van der Waals interactions to the liquid phase of the RTMS by MD simulations.

The remainder of the article is organized as follows: In the following section, we describe briefly the AMBER force field and justify our choice of atom types and force field parameters. In section 3, the results of QM and MM calculations are presented and discussed. The central part of the article is devoted to the liquid state characteristics of the RTMS as elucidated from MD simulations as reported in section 4. There, we discuss comparatively the influence of anion size and alkyl chain length in the 1-alkyl-3-methylimidazolium RTMS upon thermodynamical properties, structural features, and diffusion coefficients. We finish the article with a short conclusions in section 5.

2. Methodology and Force Field Parameters

The AMBER force field of Cornell et al.[15] employs the following functional form for the potential energy V:

$$V = \sum_{\text{bonds}} K_r(r - r_{eq})^2 + \sum_{\text{angles}} K_\theta(\theta - \theta_{eq})^2 + \sum_{\text{dihedrals}} V_n[1 + \cos(n\phi - \gamma)] + \sum_{i=1}^{N-1}\sum_{j>i}^{N}\left[\frac{A_{ij}}{R_{ij}^{12}} - \frac{B_{ij}}{R_{ij}^{6}} + \frac{q_i q_j}{R_{ij}}\right] \quad (1)$$

where the potential parameters have their usual meaning. For our computational purposes, the nonbonded Lennard-Jones parameters A_{ij} and B_{ij} were rewritten in terms of the traditional well-depth ϵ and size parameter σ:

$$A_{ij} = 4\epsilon_{ij}\sigma_{ij}^{12}$$
$$B_{ij} = 4\epsilon_{ij}\sigma_{ij}^{6} \quad (2)$$

Lennard-Jones parameters for interactions between different atom types have been obtained from the Lorentz−Berthelot mixing rule:[17]

$$\epsilon_{ij} = \sqrt{\epsilon_{ii}\epsilon_{jj}}$$
$$\sigma_{ij} = (\sigma_{ii} + \sigma_{jj})/2 \quad (3)$$

A crucial point in the parameter development consisted in the choice of the atom types. The cations EMI^+ and BMI^+ as depicted in Figure 1 exhibit the imidazolium ring representing the residue of the histidine amino acid in the protonated form. Thus, we assigned the atom types for the imidazolium ring directly to the AMBER description of this amino acid. The alkyl substituents also follow the standard AMBER atom type denomination. Figure 2 summarizes our choice of atom types for the cations.

However, this choice is not sufficient to define all of the parameters necessary for a complete force field for the cations. Because of the differences between the imidazolium ring in histidine and in the EMI^+ and BMI^+ cations, we defined a double bond between ring atoms C4 and C5 from Figure 1 turning the AMBER atom type CW into CM. Also, the connections of the alkyl substituents with the ring are not available directly from the AMBER force field but can be established taking the similar atom types N*, CK, and N* representing the atoms N1, C2, and N3, respectively, from Figure 1. By this choice of atom types, the intramolecular and

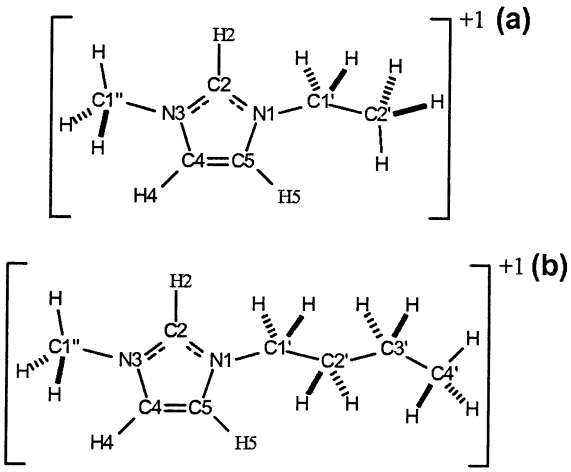

Figure 1. (a) EMI^+ atoms naming; (b) BMI^+ atoms naming.

van der Waals parameters for the cations are perfectly defined. All of these parameters are summarized in Tables 1−4.

The intramolecular potential parameters for the anions were also developed under the AMBER methodology.[16] The obtained bond stretching and bending parameters for the $AlCl_4^-$ and BF_4^- are included in Tables 1 and 2. Chlorine[16] and fluorine[18] Lennard-Jones parameters are of AMBER type, whereas the van der Waals parameters for aluminum and boron have been taken from the DREIDING force field.[19] The van der Waals parameters for the anions used in the present study are given in Table 4.

To represent the electronic charge distribution of the ions by atomic point charges, QM calculations on the ab initio level have been performed followed by the one-conformation two-stage standard RESP fitting approach.[20] The computed point charges are presented in Figure 2. To maintain the original simplicity and high performance of the MD simulations, we did not include any polarization effects in the electrostatic interaction model. Although the point charges obtained for the isolated ions do not necessarily represent the most adequate charge distribution for the condensed phase, we applied this simple model without correcting for the formation of ion pairs because of several reasons: First, a charge distribution obtained from gas-phase calculations on ion pairs cannot mimic typical condensed phase configurations involving a larger number of ions with possible partial cancellations in mutual polarization mechanisms. Second, choosing point charges obtained from gas-phase calculations on isolated ions facilitates the transferability of the charge model to the RTMS containing the same ion but another counterion. In addition, comparing Mulliken type charges for the isolated EMI^+ and $AlCl_4^-$ with results from calculations on the coordinated form, one might conclude that polarization effects are small in this class of RTMS.[6]

3. Quantum and Molecular Mechanical Calculations

QM ab initio calculations for the isolated ions were performed with the GAMESS program[21] using the UHF/6-31G(d)[22] level of theory. The procedures included the optimization of the ion structures, standard normal-mode analysis, and the electrostatic potential (ESP) grid generation for the isolated ions. This ESP grid was used to produce the RESP atomic point charges by one-conformation two-step RESP fitting with the RESP program from the AMBER package.[23]

In the atom type selection presented in the previous section, the ring atoms C4 and C5 (see Figure 1) have been defined as connected by a double bond (atom types CM). This definition

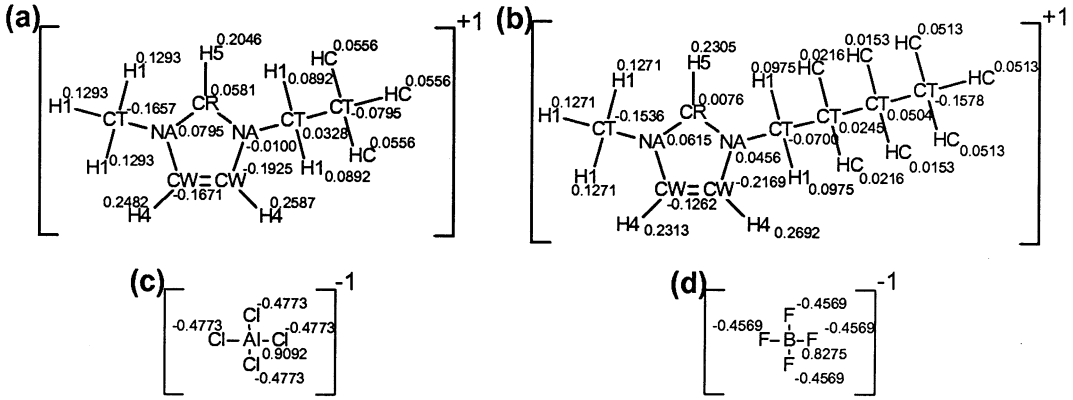

Figure 2. (a) Atom types and partial charges of EMI^+ cation; (b) Atom types and partial charges of BMI^+ cation; (c) Atom types and partial charges of $AlCl_4^-$ anion; (d) Atom types and partial charges of BF_4^- anion.

TABLE 1: Bond Stretching Potential Parameters

bond	K_r/kJ mol^{-1}Å^{-2}	r_{eq}/Å	source
CT−CT	1297.04	1.526	AMBER
CT−H1	1422.56	1.090	AMBER
CT−HC	1422.56	1.090	AMBER
CT−NA	1410.01	1.475	AMBER CT−N* bond
CR−H5	1535.53	1.080	AMBER
CR−NA	1995.77	1.343	AMBER
CW−H4	1535.53	1.080	AMBER
CW−NA	1786.57	1.381	AMBER
CW−CW	2297.02	1.350	AMBER CM−CM bond
AL−Cl	485.34	2.170	Developed here
B−F	1213.36	1.393	Developed here

TABLE 2: Bond Angle Potential Parameters

angle	K_θ/ kJ mol^{-1}rad^{-2}	θ_{eq}/ degree	source
H1−CT−H1	146.44	109.5	AMBER
H1−CT−NA	209.20	109.5	AMBER H1−CT−N* angle
CR−NA−CT	292.88	128.8	AMBER CK−N*−CT angle
CW−NA−CT	292.88	121.2	AMBER CM−N*−CT angle
CW−CW−NA	292.88	121.2	AMBER CM−CM−N* angle
CW−CW−H4	146.44	119.7	AMBER CM−CM−H4 angle
CT−CT−CT	167.36	109.5	AMBER
CT−CT−H1	209.20	109.5	AMBER
CT−CT−HC	209.20	109.5	AMBER
HC−CT−HC	146.44	109.5	AMBER
CT−CT−NA	209.20	109.5	AMBER CT−CT−N* angle
NA−CR−NA	292.88	120.0	AMBER
NA−CR−H5	146.44	120.0	AMBER
CR−NA−CW	292.88	120.0	AMBER
NA−CW−H4	146.44	120.0	AMBER
Cl−Al−Cl	209.20	109.5	Developed here
F−B−F	209.20	109.5	Developed here

is corroborated by the QM bond order for both cations as illustrated in Table 5. Furthermore, electronic resonance within the imidazolium ring is restricted to a delocalized double bond involving the atoms N1, C2, and N3. The N1−C4 and N3−C5 bonds are clearly identified as single bonds.

In addition, MM calculations were performed utilizing the Tinker package.[24] The MINIMIZE program was employed to achieve optimized molecular geometries of the isolated ions with the force field parameters presented in the previous section. Afterwards, the VIBRATE program was used to obtain the normal modes of vibration for the established force field.

Some structural parameters for the optimized geometries of the cations obtained from QM and MM calculations are compared in Tables 6−8 with experimental X-ray data.[13,14] Quite generally, the QM and MM structures are in satisfactory agreement with the X-ray data, especially if one considers that the X-ray data have been obtained from crystal structures

TABLE 3: Dihedral Torsion Potential Parameters

torsion	V_n/ kJ mol^{-1}	γ/ degree	n	source
Proper Torsions				
NA−CR−NA−CT	7.1128	180	2	AMBER X−CK−N*−X
H5−CR−NA−CT	7.1128	180	2	AMBER X−CK−N*−X
H5−CR−NA−CW	9.7278	180	2	AMBER
NA−CR−NA−CW	9.7278	180	2	AMBER
X−CT−CT−X	0.6508	0	3	AMBER
X−CT−NA−X	0	0	2	AMBER X−CT−N*−X
X−CW−CW−X	27.8236	180	2	AMBER X−CM−CM−X
CW−CW−NA−CR	7.7404	180	2	AMBER X−CM−N*−X
CW−CW−NA−CT	7.7404	180	2	AMBER X−CM−N*−X
H4−CW−NA−CR	6.2760	180	2	AMBER X−CW−NA−X
H4−CW−NA−CT	7.7404	180	2	AMBER X−CM−N*−X
Improper Torsions				
X−X−CR−H5	4.6024	180	2	AMBER
X−X−CW−H4	4.6024	180	2	AMBER
X−X−CT−NA	4.1840	180	2	AMBER CM−C−N*−CT

TABLE 4: Nonbonded Van Der Waals Potential Parameters

atom type	σ_{ii}/Å	ϵ_{ii}/kJ mol^{-1}	source
HC	2.6495	0.0657	AMBER
H1	2.4714	0.0657	AMBER
H4	2.5106	0.0628	AMBER
H5	2.4215	0.0628	AMBER
CT	3.3997	0.4577	AMBER
CR	3.3997	0.3598	AMBER
CW	3.3997	0.3598	AMBER
NA	3.2500	0.7113	AMBER
Cl	3.4709	1.1088	AMBER
F	3.1181	0.25522	AMBER
Al	3.9111	1.2970	DREIDING
B	3.5814	0.39748	DREIDING

TABLE 5: QM Bond Order Results for the Selected Bonds of the Cations

bond	EMI^+	BMI^+	bond	EMI^+	BMI^+
C1″−N3	0.78	0.78	C2−N3	1.29	1.30
C3′−C4′		0.98	N3−C4	1.06	1.05
C2′−C3′		0.97	C4−C5	1.76	1.77
C1′−C2′	0.96	0.96	C5−N1	1.06	1.06
N1−C1′	0.77	0.76	N1−N3	0.06	0.06
N1−C2	1.31	1.31			

whereas isolated cations have been treated by the calculations. Both, the QM and MM optimized geometries exhibit a planar imidazolium ring in agreement with the experimental data as becomes evident from the total internal ring angle given in Table 7. Bond lengths and angles within the imidazolium ring are very well reproduced (the maximum deviations against the experiment are 0.06 Å and 7° for both the QM and MM calculations).

TABLE 6: QM, MM, MD, and Experimental Data for Selected Bond Lengths (in Å) of the Cations

	EMI$^+$				BMI$^+$			
bond	QM	MM	MD[a]	X-ray[b]	QM	MM	MD[a]	X-ray[c]
C1″−N3	1.469	1.481	1.485	1.45	1.466	1.470	1.477	1.465
C4′−C3′					1.528	1.524	1.533	1.518
C2′−C3′					1.531	1.527	1.539	1.475
C1′−C2′	1.522	1.532	1.533	1.57	1.527	1.527	1.537	1.526
C1′−N1	1.477	1.484	1.483	1.48	1.477	1.473	1.482	1.478
N1−C2	1.314	1.349	1.351	1.31	1.314	1.339	1.348	1.332
C2−N3	1.317	1.349	1.351	1.28	1.316	1.344	1.347	1.334
N3−C4	1.377	1.382	1.382	1.39	1.378	1.386	1.380	1.369
C4−C5	1.342	1.349	1.347	1.30	1.342	1.343	1.348	1.355
C5−N1	1.377	1.384	1.384	1.42	1.378	1.387	1.381	1.373
N1−N3	2.153	2.210	n.a.	n.a.	2.153	2.196	n.a.	n.a.

[a] From MD simulations of the cation with $AlCl_4^-$ as counterion. [b] From ref 13 for crystalline EMI·$AlBr_4$. [c] From ref 14 for crystalline BMI·BPh_4.

TABLE 7: QM, MM, MD, and Experimental Data for Selected Bond Angles (in Degree) of the Cations

	EMI$^+$				BMI$^+$			
bond pair	QM	MM	MD[a]	X-ray[b]	QM	MM	MD[a]	X-ray[c]
C1″−N3−C2	125.8	130.2	130.1	125	126.5	128.2	130.0	124.9
C1″−N3−C4	126.3	122.9	122.2	128	125.6	124.7	122.5	125.9
C4′−C3′−C2′					112.2	110.0	112.0	113.7
C3′−C2′−C1′					111.6	109.4	112.1	116.1
C2′−C1′−N1	112.1	110.9	109.5	108	112.2	109.6	111.9	110.9
C1′−N1−C2	126.1	130.2	129.9	123	126.2	127.8	130.1	125.0
C1′−N1−C5	125.8	123.0	122.4	126	125.9	124.8	122.6	125.9
N1−C2−N3	109.8	110.0	109.3	108	109.9	109.8	109.9	107.9
C2−N3−C4	107.9	106.9	107.1	107	108.0	107.0	106.9	109.2
N3−C4−C5	107.1	108.2	108.0	112	107.0	108.0	108.0	106.9
C4−C5−N1	107.1	108.1	108.0	101	107.2	107.8	108.1	107.0
C5−N1−C2	108.0	106.9	107.1	111	107.9	107.3	106.7	109.0
ring total	540.0	540.0	539.5	539	540.0	540.0	539.5	540.0

[a] From MD simulation of the cation with $AlCl_4^-$ as counterion. [b] From ref 13 for crystalline EMI·$AlBr_4$. [c] From ref 14 for crystalline BMI·BPh_4.

TABLE 8: QM, MM, MD, and Experimental Data for the Main Dihedral Angles (in Degrees) of the Cations

	EMI$^+$				BMI$^+$			
dihedral	QM	MM	MD[a]	X-ray[b]	QM	MM	MD[a]	X-ray[c]
C2′−C1′−N1−C2	103.7	101.6	86.7	118.8	98.5	95.7	84.2	112.4
C2′−C1′−N1−C5	75.0	78.5	94.5	58.5	79.1	81.6	96.8	66.5

[a] From MD simulation of the cation with $AlCl_4^-$ as counterion. [b] From ref 13 for crystalline EMI·$AlBr_4$. [c] From ref 25 for crystalline 1-dodecyl-3-methylimidazolium hexafluoride.

TABLE 9: Dipole Moments (in D) with Origin at the Ion's Center of Mass from QM Calculations (μ_{QM}) and the Set of Point Charges Used in This Work (μ_{RESP}) for the Cations

ion	μ_{QM}	μ_{RESP}	absolute difference	relative deviation (%)
EMI$^+$	1.76	1.78	+0.02	+1.19
BMI$^+$	5.57	5.61	+0.04	+0.75

Small deviations are found for the alkyl bonds. Moreover, looking into the principal dihedral angles from Table 8, it becomes evident that the MM calculations reproduce the QM dihedral angles quite accurately.

Concerning the dipole moments of the cations, to our knowledge, there are no experimental data available in the literature. Thus, we compare QM dipole moments with those obtained from our set of point charges obtained within the RESP methodology as indicated in Figure 2. This comparison is illustrated in Table 9. Note that the total dipole moments for the tetrahedral anions are zero because of symmetry considerations. The EMI$^+$ cation possesses a rather small dipole moment (1.76 D) when compared with the BMI$^+$ cation (5.57 D). The EMI$^+$ molecular geometry resembles features close to the C_{2v} symmetry, whereas the center of the charge distribution in the BMI$^+$ is significantly shifted towards the larger alkyl group. Most of the larger charges appear in the imidazolium ring systems localized at the carbons C4 and C5 as well as the ring hydrogen substituents. Thus, as a consequence of the molecular symmetry, individual bond dipoles in the EMI$^+$ are expected to cancel partially others more than in the BMI$^+$. Localized larger charges at the hydrogen substituents of the carbons C2, C4, and C5 identify these hydrogen atoms as possible participants in hydrogen bonds with the anions. United atom force fields are more likely to miss details concerning these short-range intermolecular structural features.

As an additional test for the established intramolecular potential parameters, a MM normal-mode analysis for the ions has been performed. In the case of the EMI$^+$ cation[6,26] and $AlCl_4^-$ anion,[27] experimental vibrational frequencies have been published; for the BMI$^+$ and the isolated anions, we are restricted to comparing MM normal-mode frequencies with the QM findings. The EMI$^+$ frequencies are quite generally in satisfactory agreement with the experimental data with an average deviation of 45 cm^{-1}. Larger deviations were found for the ring stretching frequencies with MM normal modes overestimated up to 163 cm^{-1}. These differences are probably due to a less accurate representation for the charged EMI$^+$ ring system by the used bond parameters for the uncharged ring system of the histidine amino acid. However, we decided to maintain the coherence with the AMBER force field and with our protonated histidine approach and did not reparameterize any parameters in order to minimize the deviations between MM and experimental vibrational frequencies for the EMI$^+$ cation.

In the case of the BMI$^+$ cation, the MM normal-mode frequencies for the established force field have been compared to QM calculations. Deviations between MM and QM frequencies are of the same order as observed for the EMI$^+$ cation. Again, larger deviations in the normal-mode frequencies are originated at the vibrations involving the imidazolium ring system because of our histidine approach for the bond parameters. MM normal-mode frequencies for the $AlCl_4^-$ anion are in satisfactory agreement with experimental data[27] (average deviation: 23 cm^{-1}, maximum deviation: 73 cm^{-1}). In the case of the BF_4^- anion, larger deviations in the normal-mode frequencies obtained from MM and QM calculations have been observed (average deviation: 102 cm^{-1}, maximum deviation: 135 cm^{-1}). This larger deviations in the BF_4^- anion are probably due to its small size and quantum effects that are not well reproduced by simple harmonic models. Moreover, the definition of the anion bending constants by AMBER's standard value for the boron hybridization is probably less accurate than for larger central atoms such as carbon or nitrogen.

The presented results for the isolated ions indicate that the established force field successfully mimics the QM ion structures and its charge distributions. Although there are some minor deviations in predicting vibrational frequencies, the established force field has been applied to liquid-state simulations on the RTMS as described in the following section.

4. Liquid-State Molecular Dynamics Simulations

MD simulations were carried out with the MDynaMix program[28] and its trajectories analyzed with an especially adapted version of the TRANAL program.[28] The simulations

TABLE 10: Temperatures T (in K), Experimental Densities ρ_{exp} (in g/cm^3),[7,27,30] Simulated NpT Densities ρ_{NpT} (in g/cm^3), and Density Deviations $\Delta\rho = \rho_{exp} - \rho_{NpT}$ (in %)

RTMS	T	ρ_{exp}	ρ_{NpT}	$\Delta\rho$ (in %)
EMI·$AlCl_4$	298	1.302	1.316	1.07
EMI·BF_4	295	1.240	1.255	1.19
BMI·$AlCl_4$	298	1.238	1.229	−0.70
BMI·BF_4	303	1.170	1.174	0.33

TABLE 11: Calculated Heats of Vaporization ΔH_{vap}, Intermolecular Potential Energies U_{int}, and Its Van Der Waals U_{vdw} and Electrostatic Contributions U_{el} for the Studied RTMS[a]

RTMS	U_{el}	U_{vdw}	U_{int}	ΔH_{vap}
EMI·$AlCl_4$	−202.3 ± 4.0	−41.6 ± 0.1	−243.9 ± 4.1	246.4
EMI·BF_4	−226.7 ± 2.7	−26.7 ± 0.1	−253.4 ± 2.7	255.8
BMI·$AlCl_4$	−189.9 ± 3.6	−47.3 ± 0.1	−237.2 ± 3.7	239.7
BMI·BF_4	−218.5 ± 2.4	−31.9 ± 0.1	−250.4 ± 2.4	252.9

[a] All of the data are given in kJ/mol.

were undertaken in the *NVT* ensemble using the Nosé−Hoover thermostat[29] with a coupling constant of 30 fs. The temperature was fixed at a temperature close to 298 K, and the size of the cubic simulation box was defined in accordance with the experimental densities[7,27,30] shown in Table 10. The simulation box was composed of 128 randomly arranged ion pairs. The usual periodic boundary conditions have been applied. Equations of motion were resolved by the Tuckerman−Berne double time-step algorithm[31] with the large and short time steps kept at 2 and 0.2 fs, respectively. All the simulations were equilibrated for at least 200 ps. The production phase lasted not less than 100 ps. The liquid-state configurations were saved for further analysis in intervals of 5 time steps (10 fs). In all of the simulations, the cutoff radius was kept to 17 Å, also representing the real-space cutoff radius for Ewald Summation[17] in the employed Coulombic forces treatment.

The equilibration phase was monitored by plotting the total, kinetic, intermolecular, and intramolecular potential energies. From the following production runs, we extracted heats of vaporization (ΔH_{vap}) and internal energies (U_{int}), self-diffusion constants (D), and the several radial distribution functions (RDFs). The electrostatic (U_{el}) and van der Waals (U_{vdw}) contributions to U_{int} were also studied.

In addition, we performed constant pressure simulations (1 atm) for the RTMS within the Nosé−Hoover NpT ensemble[29] (coupling constants 400 and 30 fs, respectively). The obtained densities are compared with the experimental data in Table 10. The difference between computed and experimentally measured densities is approximately 1% for all of the studied RTMS and can be considered to be very close to the experimental imprecision in this kind of measurement.[13]

The heat of vaporization has been computed from the average intermolecular energy by

$$\Delta H_{vap} = -U_{int} + RT \tag{4}$$

where R represents the gas constant. Simulated values for ΔH_{vap} and internal energies are compiled in Table 11. Experimental heats of vaporization are not available because of the low volatile character of the RTMS. The obtained values for ΔH_{vap} are of the same magnitude as in molten metals (aluminum, 294 kJ/mol; gold, 324 kJ/mol[32]) and inorganic salts (silver chloride, 198 kJ/mol; cadmium fluoride, 214 kJ/mol[32]), and significantly higher than in some low-volatile organic compounds (1-tetradecaneol, 102.2 kJ/mol at 298 K[32]). Although the lack of experimental data does not permit a quantitative comparison, one might conclude that the simulations reproduce the experimentally observed nonvolatile behavior of the RTMS. Moreover, looking into the electrostatic and van der Waals contributions to the intermolecular interaction energy U_{int}, as shown in Table 11, it becomes evident that the electrostatic interaction energy represents by far the dominant contribution to U_{int}. This is probably the main explanation for most of the physical properties in this class of RTMS.

Also from the data in Table 11, it can be seen that changing the anion from $AlCl_4^-$ to BF_4^- comes along with increasing ΔH_{vap} because of the larger electrostatic contribution in the BF_4^- containing liquids. As expected, the size effect in the cations produces larger van der Waals interactions in RTMS containing the butyl substituent. However, the electrostatic interactions show the opposite trend producing smaller heats of vaporization for the butyl substituted cations.

From Tables 6 and 7, it becomes evident that the bond lengths and bond angles in the liquid-state remain close to the values obtained by the MM calculations. In the dihedral angles given in Table 8, some differences between the liquid-state simulations and the MM calculations are found. Note that the bond lengths and angles involving the ring system are almost constant. Thus, possibly, the imidazolium ring might be treated as rigid in the simulations.

The self-diffusion constant D has been obtained from the mean-square displacement[17] for the ions:

$$D = \frac{1}{6t}\langle[\boldsymbol{r}(t_0 + t) - \boldsymbol{r}(t_0)]^2\rangle \tag{5}$$

with t_0 representing some initial time. Several time origins t_0 have been chosen along the trajectory. In addition, the x, y, and z components from eq 5 have been analyzed independently. Quite generally, the expected linear behavior in the mean-square displacement was observed for times larger than 5 ps for all trajectory pieces and directions. An error of approximately $\pm 0.8 \times 10^{-7}$ cm^2/s was estimated in the calculated diffusion constants.

TABLE 12: Calculated Self-Diffusion Constants D (in 10^{-7} cm^2/s) for the Cations (D_+) and Anions (D_-)

RTMS	D_+	D_-	RTMS	D_+	D_-
EMI·$AlCl_4$	8.2	5.9	EMI·BF_4	1.5	1.1
BMI·$AlCl_4$	3.4	3.5	BMI·BF_4	1.2	1.0

The calculated self-diffusion constants for the cations and anions are summarized in Table 12. An experimental value, $D = 9.5 \times 10^{-7}$ cm^2/s at 293 K, for the EMI^+ cation in EMI·$AlCl_4$ has been determined by NMR techniques[33] and agrees reasonably well with the simulated value of 8.2×10^{-7} cm^2/s.[34] The small difference between experiment and simulation ($\simeq 1.4 \times 10^{-7}$ cm^2/s) might be improved by more extensive simulations in order to achieve the best results.[35]

Tables 12 gives us some other insights. First, the cation and the anion self-diffusion constants in each liquid are very similar. Also, the anion effect can be noticed by the reduction of the diffusion constants when the $AlCl_4^-$ is substituted by BF_4^-. This observation can be explained because of an increase in the packing of the ions in the liquids containing the small anion. Finally, the increase in the size of the ring alkyl substituents from ethyl to butyl comes along with a reduction of the diffusion constants. This effect can be associated with a restriction of free space among the ions caused by the alkyl size change.

A preliminary description of some general structural features of the RTMS has been acquired from radial pair distribution functions $g(r)$. To compute comparable RDFs in the different ionic liquids, we have defined the geometric center of the

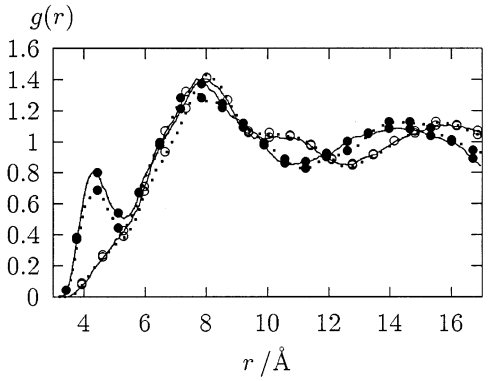

Figure 3. RDFs for the geometric centers of the imidazolium ring systems. Full line with ○, EMI·$AlCl_4$; dotted line ○, BMI·$AlCl_4$; full line with ●, EMI·BF_4; dotted line with ●, BMI·BF_4.

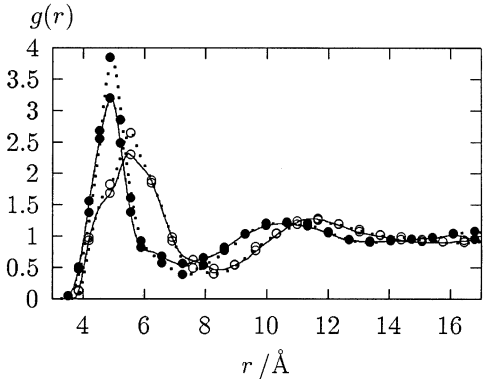

Figure 4. Same as in Figure 3 but for pairs formed by the geometric center of the imidazolium ring system and the anion's central atom.

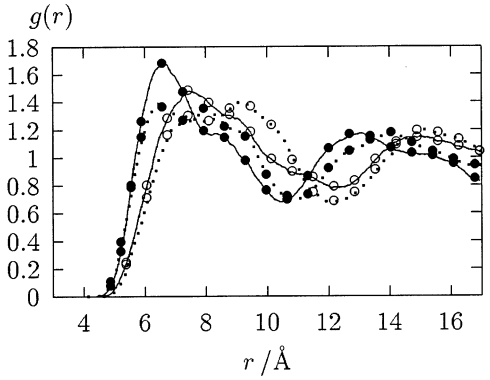

Figure 5. Same as in Figure 3 but for the central atoms of the anions.

imidazolium ring as the point of reference in the cations. The natural reference in the anions is represented by the central atom. The three RDFs for distances between these reference sites have been computed for the four ionic liquids. The obtained $g(r)$ are illustrated in Figures 3−5. These simple RDFs are quite difficult to interpret, and as noted earlier in ref 9, deeper studies involving spatial distribution functions are necessary to obtain more detailed structural information about packing characteristics, hydrogen bonding, etc. However, the simple RDFs enable us to extract some influences of the different cations and anions on the liquid structure of the RTMS.

Concerning the environment of the cations, the Figures 3 and 4 demonstrate that the local structural features are strongly affected by the nature of the anion. The cation−cation RDF from Figure 3 shows that a short distance shoulder between 4 and 5 Å of the first peak in the $g(r)$ for the $AlCl_4^-$ containing RTMS turns into a clear pre-peak in the $g(r)$ for the BF_4^- based RTMS.

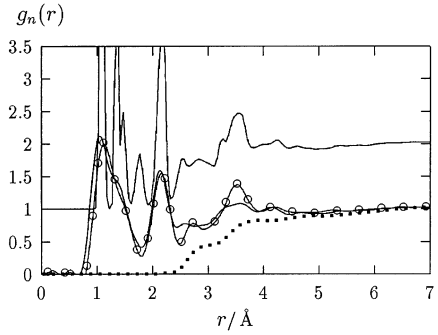

Figure 6. Neutron scattering pair distribution function $g_n(r)$ from eq 6 as obtained from the simulation (full line, shifted by 1) and from experiment (full line, not shifted). Also illustrated: the fast Fourier broadened simulated $g_n(r)$ (full line with ○) and the intermolecular contribution to $g_n(r)$ (dotted line).

The peak position and height of the first maximum in these $g(r)$ is very similar with a long range shoulder appearing only in the RTMS with $AlCl_4^-$ at almost 11 Å. On the other hand, the size of the cation's alkyl group is only weakly reflected in the $g(r)$ for the geometric centers of the imidazolium ring system.

The cation−anion RDFs depicted in Figure 4 clearly indicate the size effect of the anions. The peak positions in the $g(r)$ for the BF_4^- based RTMS are dislocated by approximately 0.5 Å towards smaller distances when compared to the $AlCl_4^-$ systems. The first peak in the $AlCl_4^-$ RTMS is significantly broadened with a short range shoulder corresponding to the maximum position of the $g(r)$ for the BF_4^- ionic liquids. The larger alkyl group in the BMI^+ cations produces a higher first peak and a lower first minimum than the ethyl substituted cations indicating a more defined first solvation sphere of anions around the cations and vice versa in the BMI^+ based RTMS.

The anion−anion $g(r)$ in Figure 5 also present the anion's size effect. The $g(r)$ calculated from the BF_4^- RTMS exhibit more short-range character than the $g(r)$ obtained for $AlCl_4^-$ pairs. All of the anion−anion RDFs present very broad first maxima possessing more or less pronounced long range shoulders. In addition, these RDFs for anion pairs present some influence of the alkyl group in the cations. The $g(r)$ for the BMI^+ based ionic liquids are slightly shifted toward larger distances, especially at distances corresponding to regions beyond the first maxima.

In the case of deuterated EMI·$AlCl_4$, experimental liquid state neutron diffraction data have been recently published.[7] The experimental neutron diffraction RDF, $g_n(r)$, can be computed as a weighted superposition of all the atom−atom pair distribution functions $g_{ij}(r)$

$$g_n(r) = \frac{\sum_{ij} x_i x_j b_i b_j g_{ij}(r)}{(\sum_i x_i b_i)^2} \qquad (6)$$

where the b_i and b_j represent the neutron scattering cross sections[36] for atoms i and j with atomic mole fraction x_i and x_j. We have calculated the neutron diffraction RDF from all of the atom−atom RDFs[10] by eq 6 and compare the computed $g_n(r)$ with the experimental data in Figure 6.

In addition to the simulated and the experimental $g_n(r)$, we also illustrate in Figure 6 the calculated intermolecular contribution and a fast Fourier broadened curve of the calculated total

$g_n(r)$. Comparing the simulated and smoothed $g_n(r)$ with the experimental result, one might notice the remarkable agreement between the two data sets, not only in the peak positions but also in their amplitudes and shapes. A significant deviation between experimental and simulated $g_n(r)$ is found at distances between 3.6 and 3.8 Å, where the calculated $g_n(r)$ exhibit a rather intense peak not present in the experimental data. This peak has been traced back to the intermolecular Cl−Cl contribution of the $AlCl_4^-$ anions. The experimental observation of cluster formation ($Al_2Cl_7^-$, $Al_3Cl_{10}^-$, etc.) in molten chloroaluminates[37] cannot be reproduced by our model for the $AlCl_4^-$ anion used in the simulations. However, one might certainly expect a broader distribution of Cl−Cl distances in the real system due to this type of cluster formation and decomposition.

Comparing the experimental $g_n(r)$ with the calculated intermolecular contribution, it becomes evident that all amplitudes below 2 Å are originated at intramolecular distances. In our preliminary communication,[10] we have assigned the first intermolecular contributions to hydrogen−chloro pairs at distances of approximately 2.8 Å indicating hydrogen bonds between the imidazolium ring hydrogens and the anions.

5. Conclusions

In the present article, we present the parametrization of a force field and its validation for the liquid state description of four simple RTMS containing the 1-alkyl-3-methylimidazolium cation. The parametrization process followed most of the techniques involved in the development of the AMBER force field. The lacking van der Waals parameters for the aluminum and boron atoms were taken directly from the DREIDING force field. Analogies between the imidazolium ring in the protonated histidine and in the dialkylimidazolium cations were used to establish the maximum number of parameters for the ring system from the original AMBER force field.[15]

The proposed force field for the RTMS was validated against available experimental properties (density, self-diffusion constant, X-ray crystal data, and liquid state neutron diffraction). Quite generally, we have achieved a very good agreement between simulated results and experimental findings indicating that the developed strategy of parametrization might be extended to other RTMS, especially for ionic liquids based on the dialkylimidazolium cation.

A detailed analysis of the structural features for the four ionic liquids studied in this article is underway and represents the main subject of a forthcoming paper.

In summary, the successful parametrization of the RTMS encourages us to extend the procedure in order to include other important cations and anions and to investigate their influences on structure, hydrogen bonding, solvent-to-solute interactions, and other physical properties, both in the bulk liquid and in mixtures with other solvents (even other green solvents, like supercritical CO_2 and perfluorinated solvents). Finally, the systematic study of the RTMS might lead to a better understanding of its structure−activity relationship that afterwards might interfere in the improvement of their unique and desirable properties.

Acknowledgment. Financial support from the Brazilian agencies CNPq (process 521628/97-0) and FAPERGS (process AUX 00/0902.7), as well as the grants for J.d.A. and E.S.B. from CAPES are gratefully acknowledged. We thank J. Caldwell and M. Froeyen for their help on RESP charge fitting from GAMESS results as well as A. Laaksonen and A. P. Lyubartsev for providing the MDynaMix and TRANAL programs with some initial guidelines. J. Ponder is also acknowledge for useful suggestions on the TINKER Package. Stimulating discussions with P. A. Netz and J. Dupont have also contributed to the present work.

References and Notes

(1) Bolm, C.; Beckmann, O.; Dabard, O. A. G. *Angew. Chem.* **1999**, *111*, 957; *Angew. Chem., Int. Ed. Engl.* **1999**, *38*, 907.

(2) Kaupp, G. *Angew. Chem.* **1994**, *106*, 1519; *Angew. Chem., Int. Ed. Engl.* **1994**, *33*, 1452. Jessp, P. G.; Ikariya, T.; Noyori, R. *Chem. Rev.* **1999**, *99*, 475.

(3) Fish, R. H. *Chem. Eur. J.* **1999**, *5*, 1677.

(4) Dupont, J.; Consorti, C. S.; Spencer, J. *J. Braz. Chem. Soc.* **2000**, *11*, 337.

(5) Suarez, P. A. Z.; Einloft, S.; Dullius, J. E. L.; de Souza, R. F.; Dupont, J. *J. Chim. Phys.* **1998**, *95*, 1626. Welton, T. *Chem. Rev.* **1999**, *99*, 2071. Wasserscheid, P.; Keim, W. *Angew. Chem., Int. Ed.* **2000**, *39*, 3772.

(6) Takahashi, S.; Curtiss, L. A.; Gosztola, D.; Koura, N.; Saboungi, M.-L. *Inorg. Chem.* **1995**, *34*, 2990.

(7) Takahashi, S.; Suzuya, K.; Kohara, S.; Koura, N.; Curtiss, L. A.; Saboungi, M.-L. *Z. Phys. Chem.* **1999**, *209*, 209.

(8) Dymek, C. J., Jr.; Stewart, J. J. P. *Inorg. Chem.* **1989**, *28*, 1472. Wilkes, S. J.; Lewisky, J. A.; Wilson, R. A.; Hussey, C. L. *Inorg. Chem.* **1982**, *21*, 1263. Meng, Z.; Dölle, A.; Carper, W. R. *J. Mol. Struct. (THEOCHEM)* **2002**, *585*, 119.

(9) Hanke, C. G.; Price, S. L.; Lynden-Bell, R. M. *Mol. Phys.* **2001**, *99*, 801.

(10) de Andrade, J.; Böes, E. S.; Stassen, H. *J. Phys. Chem. B* **2002**, *106*, 3546.

(11) Hanke, C. G.; Atamas, N. A.; Lynden-Bell, R. M. *Green Chem.* **2002**, *4*, 107.

(12) Shah, J. K.; Brennecke, J. F.; Maginn, E. J. *Green Chem.* **2002**, *4*, 112.

(13) Elaiwi, A.; Hitchcock, P. B.; Seddon, K. R.; Srinivasan, N.; Tan, Y.-M.; Welton, T.; Zora, J. A. *J. Chem. Soc., Dalton* **1995**, 3467.

(14) Dupont, J.; Suarez, P. A. Z.; de Souza, R. F.; Burrow, R. A.; Kintzinger, J.-P. *Chem. Eur. J.* **2000**, *6*, 2377.

(15) Cornell, W. D.; Cieplak, P.; Bayly, C. I.; Gould, I. R.; Merz, K. M., Jr.; Ferguson, D. M.; Spellmeyer, D. C.; Fox, T.; Caldwell, J. W.; Kollman, P. A. *J. Am. Chem. Soc.* **1995**, *117*, 5179.

(16) Fox, T.; Kollman, P. A. *J. Phys. Chem. B* **1998**, *102*, 8070.

(17) Allen, M. P.; Tildesley, D. J. *Computer Simulations of Liquids*; Clarendon Press: Oxford, 1987.

(18) Gough, C. A.; DeBolt, S. E.; Kollman, P. A. *J. Comput. Chem.* **1992**, *13*, 963.

(19) Mayo, S. L.; Olafson, B. D.; Goddard, W. A., III. *J. Phys. Chem.* **1990**, *94*, 8897.

(20) Bayly, C. I.; Cieplak, P.; Cornell, W. D.; Kollman, P. A. *J. Phys. Chem.* **1993**, *97*, 10269.

(21) Schmidt, M. W.; Baldridge, K. K.; Boatz, J. A.; Elbert, S. T.; Gordon, M. S.; Jensen, J. J.; Koseki, S.; Matsunaga, N.; Nguyen, K. A.; Su, S.; Windus, T. L.; Dupuis, M.; Montgomery, J. A. *J. Comput. Chem.* **1993**, *14*, 1347.

(22) Hariharan, P. C.; Pople, J. A. *Theor. Chim. Acta* **1973**, *28*, 213; Francl, M. M.; Pietro, W. J.; Hehre, W. J.; Binkley, J. S.; Gordon, M. S.; DeFrees, D. J.; Pople J. A. *J. Chem. Phys.* **1982**, *77*, 3654.

(23) Case, D. A.; Pearlman, D. A.; Caldwell, J. W.; Cheatham, T. E., III; Ross, W. S.; Simmerling, C. L.; Darden, R. A.; Merz, K. M.; Stanton, R. V.; Cheng, A. L.; Vincent, J. J.; Crowley, M.; Tsui, V.; Radmer, R. J.; Duan, Y.; Pitera, J.; Massova, I.; Seibel, G. L.; Singh, U. C.; Weiner, P. K.; Kollman, P. A. *AMBER 6*; University of California: San Francisco, CA, 1999.

(24) Pappu, R. V.; Hart, R. K.; Ponder, J. W. *J. Phys. Chem. B* **1998**, *102*, 9725. Dudek, M. J.; Ramnarayan, K.; Ponder, J. W. *J. Comput. Chem.* **1998**, *19*, 548.

(25) Gordon, C. M.; Holbrey, J. D.; Kennedy, A. R.; Seddon, K. R. *J. Mater. Chem.* **1998**, *8*, 2627.

(26) Campbell, J. L. E.; Johnson, K. E.; Torkel, J. R. *Inorg. Org.* **1994**, *33*, 3340.

(27) Hagiwara, R.; Ito, Y. *J. Fluor. Chem.* **2000**, *105*, 221.

(28) Lyubartsev, A. P.; Laaksonen, A. *Comput. Phys. Comm.* **2000**, *128*, 565.

(29) Martyna, G. J.; Tuckerman, M. E.; Tobias, D. J.; Klein, M. L. *Mol. Phys.* **1996**, *87*, 1117. Nosé, S. *Mol. Phys.* **1984**, *52*, 255.

(30) Fannin, A. A., Jr.; Floreani, D. A.; King, L. A.; Landers, J. S.; Piersma, B. J.; Stech, D. J.; Vaughn, R. L.; Wilkes, J. S.; Williams, J. L. *J. Phys. Chem.* **1984**, *88*, 2614.

(31) Tuckerman, M.; Berne, B. J. *J. Chem. Phys.* **1992**, *97*, 1990.

(32) Lide, D. R., Ed. *Handbook of Chemistry and Physics*, 80th ed; CRC Press: Boca Raton, FL, 1999−2000.

(33) Larive, C. K.; Lin, M.; Piersma, B.; Carper, W. R. *J. Phys. Chem.* **1995**, *99*, 12409.

(34) In our preliminary communication,[10] we published the numerical value of 11.6×10^{-7} cm^2/s as the diffusion constant for the EMI cation. Additional trajectory analysis has shown that this value has been slightly overestimated in ref 10.

(35) Chitra, R.; Yashonath, S. *J. Phys. Chem. B* **1997**, *101*, 5437.

(36) Hughes, D. J.; Harvey, J. A. *U.S. Atomic Energy Comission-Neutron Cross Sections*; McGraw-Hill: New York, 1955.

(37) Tosi, M. P.; Price, D. L.; Saboungi, M. L. *Annu. Rev. Phys. Chem.* **1993**, *44*, 173. Akdeniz, Z.; Tosi, M. P. *Z. Naturforsch. A* **1999**, *54*, 180.